SECTION 3

ELECTRICAL AND OPTICAL CHARACTERIZATION

3.1 ELECTRICAL CHARACTERIZATION

3.1.1 Introduction

3.1.2 Indium Selenide

3.1.3 Indium Telluride

3.1.4 Indium Sesquitelluride

3.1.5 Copper Indium Diselenide

3.2 OPTICAL CHARACTERIZATION

3.2.1 Introduction

3.2.2 Indium Selenide

3.2.3 Indium Telluride

3.2.4 Indium Sesquitelluride

3.2.5 Copper Indium Diselenide

3.1 ELECTRICAL CHARACTERIZATION

3.1.1 Introduction

The electrical and optical properties of semiconductor thin films are profoundly influenced by minute quantities of structural and chemical imperfections, which in turn are controlled by the detailed preparative and growth conditions. Conversely, electrical and optical measurements can be used to characterize with great sensitivity the defect structure of thin films. But the measurements by themselves usually reveal nothing of the qualitative nature of the defects. This can only be inferred by tracing their behaviour through systematic variations, for example, in preparative conditions, annealing experiments, or the gaseous environment.

Semiconductor thin films have been studied with much attention and interest for their device applications. The current transport properties of these films may be characterized by the resistivity, Hall coefficient and Hall mobility, nature and density of charge carriers. A study of the temperature dependence of these parameters is generally essential to an understanding of the carrier-scattering mechanisms responsible for these transport properties.

The resistivity of amorphous films is significantly higher than that of the crystalline films(80-82). However, compared to the small temperature dependence of the resistivity of crystalline films, amorphous films show a change in resistivity by several orders over a small range of temperature. The log resistivity versus reciprocal temperature plots show a continuously variable slope yielding an activation energy in a wide range. Measurements of Hall effect in amorphous and high resistivity materials are very difficult and uncertain. However, crude measurements suggest that the density of carriers remain essentially same in both amorphous and crystalline structures but the changes in the transport properties result from variations in the mobility of the carriers (80, 82). Theoretical studies on the band structure

and electrical conduction in amorphous conductors (82-84) reveal that even though long-range order is not preserved in an amorphous material, the features of the energy-band model are preserved, provided the molecular bonds are not significantly disturbed. The optical studies also suggest that the band structure is sufficiently well defined in the amorphous films (82).

During the course of present study, no attempt was made to study Hall mobility in the films. The nature of charge carriers was determined by the hot probe technique and detailed measurements were carried out on the electrical conductivity and its temperature dependence using conventional DC methods.

The electrical conductivity is seen to exhibit an exponential variation with temperature. The variation in conductivity with temperature can be described by the relation,

$$\sigma = \sigma_o \exp(-\Delta E/kT)$$

where σ_o is the pre-exponential factor and ΔE is the activation energy for conduction.

3.1.2 Indium Selenide

As-deposited films of indium selenide are amorphous and selenium rich as mentioned in section 2. The excess

selenium gives the films p-type nature which is confirmed by the hot probe technique. The electrical DC conductivity was measured on the deposited films in vacuum during heating and cooling cycles. The maximum temperature reached is increased by 50 K in each heating cycle. This resulted in an increase in the room temperature conductivity in the initial heating cycles as a consequence of the annealing out of some of the grown-in defects. After a few heating and cooling cycles in the temperature range 300 to 550 K, the variation of conductivity with temperature was reproducible.

Figure 3.1 shows the variation of log σ with reciprocal temperature. The activation energy calculated for the low temperature and high temperature regions are 0.26 and 0.51 eV respectively and are attributed to extrinsic and intrinsic conduction processes.

3.1.3 Indium Telluride

The electrical chacteristics of indium telluride films showed variation of conductivity with temperature identical to that of indium selenide. The films were either p-type or n-type depending on the composition of the bulk starting material and the deposition conditions. A slight excess of tellurium in the grown films makes them p-type while films which are deficient in tellurium

are n-type. In the present investigation, p-InTe films were prepared for the fabrication of nickel-indium telluride schottky barrier junctions. The electrical characterization of p-InTe is given here. The films were subjected to heating and cooling cycles in the temperature range 300 to 400 K in order to avoid the possibility of re-evaporation of the constituent elements leading to off-stoichiometry at elevated temperature. This temperature range was selected after detailed structural and compositional analysis of the deposited films (described in section 2).

The variation of log σ with reciprocal temperature is shown in figure 3.2. The activation energy for the extrinsic and intrinsic regions calculated from the plot are 0.23 and 0.48 eV respectively.

3.1.4 Indium Sesquitelluride

As-deposited films of indium sesquitelluride were poorly crystalline and tellurium-rich explaining the p-type nature of the films. Figure 3.3 shows the variation of conductivity with reciprocal temperature in the temperature range 300-423 K. The low temperature region of extrinsic conductivity with an activation energy of 0.23 eV is attributed to the excess tellurium content in

the films (46, 48). The high temperature region has a characteristic activation energy of 0.41 eV which does agree with the reported band gap for In_2Te_3. The curve shows another discontinuity in slope at temperatures above 473K with a high value of activation energy 0.78eV, which cannot be attributed to In_2Te_3 compound. The high value of activation energy observed in the present case can possibly suggest more than one conduction band minima in the band structure of the material, or due to indium rich surface after heating (85, 86).

3.1.5 Copper Indium Diselenide

As-deposited films of copper indium diselenide obtained by flash evaporation of stoichiometric bulk compound show n-type conduction which is attributed to excess indium content in the films as revealed by the chemical analysis. Figure 3.4 shows the variation of conductivity with temperature for a representative sample. The activation energy calculated for the low and high temperature regions are 0.13 and 0.45 eV respectively. There are marked differences in the reported values for the activation energy in the high temperature region. The differences have been attributed to the variations in the composition of the films (87). The extrinsic conductivity observed at low temperatures is again attributed to compositional variations resulting in the generation of lat-

tice defects (88). A change from n-type to p-type conduction has been observed to result from annealing and deposition at high substrate temperatures as reported by Elliott et al (4).

3.2 OPTICAL CHARACTERIZATION

3.2.1 Introduction

The most direct and perhaps the simplest method for probing the band structure of semiconductors is to study the absorption spectrum. In the absorption process, an incident photon of known energy excites an electron from a lower to a higher energy state. An analysis of the spectral dependence of absorption reveals much information about the distribution of electron energy states in the given material.

The observed absorption is usually a sum of various absorption processes possible in a given sample. The fundamental absorption refers to band-to-band transition. Excitation of an electron from the valence band to the conduction band will result in a rapid rise in the absorption and absorption edge provides a measure of the energy gap of the semiconductor. However, since the transitions are subjected to certain selection rules, the estimation of the energy gap from the absorption edge is not

a straight forward process. The spectral dependence of the absorption coefficient α can be described by the relation,

$$\alpha h\nu = A\ (h\nu - E_g)^m$$

where $h\nu$ is the energy of the incident photon, A is a constant which depends on the material and the nature of transition, E_g represents the band gap energy and m is an exponent whose value is characteristic of the nature of transition. The possible transitions are direct or phonon assisted excitations which are allowed or forbidden by the quantum selection rules, exciton absorption, transition between a band and an impurity level, transition between band tails and free carrier absorption.

In the present study, detailed analysis has been carried out to identify the nature of absorption and to evaluate the characteristic energy of transition. The study also includes the effect of deposition and post-deposition treatments on the absorption process.

3.2.2 Indium Selenide

The variation of α with the incident photon energy for as-deposited amorphous InSe film is shown in figure 3.5. The absorption curve indicates that the total absorption spectrum must be due to several optical tran-

sitions. An analysis of spectrum showed that the absorption at the fundamental edge can be described by the relation,

$$\alpha h\nu = B\,(h\nu - E_g)^2 \qquad .. \quad (1)$$

where B is a parameter that depends on the transition probability and E_g is the characteristic of an indirect allowed transition with an energy width of 0.96 eV (Fig. 3.6). The variation of α with the energy of the incident radiation can be explained satisfactorily using equation (1) upto an energy of about 1.4 eV beyond which the absorption shows characteristics of an allowed direct transition as per the equation,

$$\alpha h\nu = B'\,(h\nu - E_g')^{1/2} \qquad .. \quad (2)$$

The energy of transition E_g calculated from the plot of $(\alpha h\nu)^2$ versus $h\nu$ (Fig. 3.6) is 1.32 eV.

The indirect band gap of 0.96 eV obtained by optical absorption measurements here is in good agreement with that computed from the electrical conductivity data as well as other reported values for amorphous indium selenide films. However, there are reported values (76) of the band gap varying from 1.2 eV to 1.32 eV (14, 22) for InSe single crystals (89-91). Similar obsevations on the presence of direct as well as indirect transitions

have been reported on cadmium telluride (92), tungsten diselenide (93), copper indium sulphide (94) and cadmium indium sulphide (95).

For photon energies $h\nu \geq 1.8$ eV, the obseved absorption coefficient was more than that calculated assuming the values of B' and E_g' in equation (2). This additional absorption at higher energies is attributed to the presence of excess selenium in the films. The additional absorption may be computed as,

$$\bar{\alpha} = (\alpha_{obs.} - \alpha_{com.})$$

where $\alpha_{obs.}$ and $\alpha_{com.}$ correspond to the absorption coefficients observed and computed using equation (2) respectively. The variation of $\bar{\alpha}$ with the photon energy $h\nu \geq 1.8$ eV was found to follow the relation,

$$\bar{\alpha} h\nu = \bar{B} (h\nu - E_g')^{1/2} \quad .. \quad (3)$$

which is characteristics of an allowed direct transition with an energy of transition 2.04 eV (Fig. 3.7). This agrees well with the data reported for selenium (96). It may be added here that the chemical analysis of the deposited films indicated the presence of excess selenium (section 2).

Figure 3.8 shows the optical absorption coefficient α as a function of incident energy $h\nu$ for as-deposited

as well as that for annealed sample. Analysis of the spectra showed (Fig. 3.9) that the fundamental absorption edge can be described by the relation,

$$\alpha h\nu = B\ (h\nu - E_g)^2 \qquad .. \quad (1)$$

where B is a parameter that depends on the transition probability and E_g is the characteristic energy of transition. The dependence is characteristic of an indirect allowed transition and the corresponding energies of transition for as-deposited and annealed samples is given in table 3.1. It is observed that the indirect band gap energy as calculated from the above data increases with heat treatment. Further, it is observed that the equation (1) holds good in the lower energy region, i.e., for incident photon energy $h\nu \leqslant 1.6$ eV, beyond which the absorption follows the characteristics of an allowed direct transition according to the relation,

$$\alpha h\nu = B\ (h\nu - E_g)^{1/2} \qquad .. \quad (2)$$

The energy of transition E_g calculated from plots of $(\alpha h\nu)^2$ versus $h\nu$ (Fig. 3.10) for the as-deposited and annealed samples is given in table 3.1.

It is observed from table 3.1 that the optical energy gap, both for direct and indirect transition, increases with annealing. This increase in the energy gap seems to

have arisen from an improvement in the crystallinity with annealing. Electron microscopy studies and energy dispersive analysis of X-rays have revealed that as-deposited films are essentially amorphous in nature and selenium rich. Amorphous to crystalline transition could be brought about by vacuum annealing of the as-deposited films at a temperature of 538 K for a period of 5 hours. The films obtained after annealing at 538 K consisted of homogeneous and stoichiometric InSe phase.

3.2.3 Indium Telluride

The variation of α with the incident photon energy is shown in figure 3.11. The absorption curve is due to several optical transitions. An analysis of the spectrum showed that the absorption at the fundamental edge can be described by direct allowed transition dependence (Fig. 3.12). There is an additional absorption at higher energies beyond fundamental absorption edge which can be described by allowed indirect transition after removing the effects of direct absorption (Fig. 3.13). The results are shown in table 3.2. Both direct and indirect transition energy gap increase with the increase in annealing temperature. The observed values for indirect transition is in agreement with the results reported by Sastry et al (14).

From table 3.2, it may be noted that the absorption depends on the temperature of heat treatment, and a shift of the absorption curves occurs towards higher energy side, which may be due to gradual annealing of defects in the process of heat treatment.

The films prepared at higher substrate temperatures also show absorption due to direct and indirect transition. The results are shown in table 3.2. It may be noted that a shift of absorption curves occurs towards lower energy side (Fig. 3.14) at a substrate temperature of 473 K. The shift of the optical absorption towards lower energy (Figs. 3.15, 3.16) may be visualised as similar to "photo darkening". A red shift of the absorption edge is known to be caused by a change in the inter band correlation from positive to negative (97). The structural changes produced at higher substrate temperature may be associated with a change in the inter band correlation. The reduction in the optical gap (97) is found to be ressponsible for the increase in the absorption coefficient and for the shift of the absorption edge towards the lower energy side (98, 99).

3.2.4 Indium Sesquitelluride

Figure 3.17 shows the optical absorption of as-deposited In_2Te_3 thin films deposited at various substrate

temperatures. The films deposited at 300 K show a gradual increase in the absorption coefficient with the photon energy whereas the films deposited at higher substrate temperature show an absorption minimum in the curve. It is observed that when deposited at temperatures above 400 K, the curves exhibited an energy range in which the absorption was negligibly small. This range of transparency of the films was dependent on the temperature of deposition (Fig. 3.17). The existance of a region of complete optical transparency may be explained on the basis of the defective structure and presence of stoichiometric vacancies in the ordered phase of In_2Te_3. The intrinsic absorption edge for these films were examined using the relation given by Bardeen et al (100) which states that the absorption coefficient α is related to the incident photon energy as per the equation,

$$\alpha h\nu = B\ (h\nu - E_g)^{1/2}$$

where E_g is the energy band gap for a direct allowed transition. A plot of $(\alpha h\nu)^2$ against $h\nu$ was found to be a straight line for the films deposited at all substrate temperatures (Fig.3.18). The intercepts of these straight line plots on the energy axis at $(\alpha h\nu)^2 = 0$ were calculated to represent the band gap energies at the different substrate temperatures. These results are summarized in

table 3.3. It is observed that the band gap energy calculated assuming a direct transition for the films deposited in the temperature range 300 to 600 K is in agreement with the reported data. At substrate temperatures above 600 K, the band gap energy is observed to increase. This increase is attributed to the formation of an InTe phase in the deposits resulting from the re-evaporation of tellurium at elevated temperatures (78, 101). This view has been confirmed by structural and compositional analyses carried out on films deposited at various substrate temperatures (section 2).

3.2.5 Copper Indium Diselenide

Figure 3.19 shows the typical variation of absorption coefficient α with photon energy $h\upsilon$. The analysis of the absorption coefficient shows that the rise of α in the energy range $h\upsilon \lesssim 1.15$ eV is due to an allowed direct transition described by (102),

$$\alpha h\upsilon = A\ (h\upsilon - E_g)^{1/2}$$

with a gap energy E_g = 1.05 eV (Fig. 3.20). This gap energy is in very good agreement with direct gap energies reported by other workers (103-106).

The films show another absorption at $h\upsilon \gtrsim 1.15$ eV,

which may be due to a forbidden direct transition characterized by (102, 107),

$$\alpha h\upsilon = A\ (h\upsilon - E_g)^{3/2}$$

or to an indirect transition described by (102, 107),

$$\alpha h\upsilon = A\ (h\upsilon - E_g)^{2}$$

The corresponding energies were found to be 1.35 eV and 1.25 eV respectively (Fig. 3.21).

These results are in agreement with the conclusion of Parkers et al (108), that the absorption behaviour of $CuInSe_2$ above the fundamental edge can be understood by the existence of two optical absorptions. Such a possibility is not excluded by existing band structure calculations (109, 110), even though it seems to be well established (102-104, 111-113) that $CuInSe_2$ is a direct gap semiconductor with a gap energy of about 1.0 eV. This point of view is supported by luminescence measurements (114). But the energy band structure of $CuInSe_2$(7) predicts forbidden direct transitions caused by transitions between the copper d states in the valence bands and the s-states in conduction band. Because of this we attribute the additional absorption to a forbidden direct transition. The presence of such a forbidden direct

transition in $CuInSe_2$ has also been detected in films grown by flash evaporation (57) and DC Sputtering (115).

Table 3.1

Variation of Band Gap Energies of Direct and Indirect Transitions for As-deposited and Annealed InSe Films.

Nature of transition	Band Gap Energy eV		
	As-deposited	Annealed	
		T_a = 423 K	T_a = 473 K
Indirect	1.09	1.15	1.18
Direct	1.35	1.45	1.53

Table 3.2

Variation of Band Gap Energies of Direct and Indirect Transitions for As-deposited and Annealed InTe Films.

Nature of transition	Band Gap Energy eV					
	T_d = 300 K	T_a = 473 K	T_a = 373 K	T_d = 373 K	T_d = 473 K	T_d = 573 K
Direct	0.690	0.725	0.850	1.075	0.935	1.050
Indirect	0.975	1.060	1.180	1.160	1.065	1.145

Table 3.3

Variation of Band Gap Energies of Direct Transitions for In_2Te_3 Film Deposited at Various Substrate Temperature.

Deposition Temperature T, K	Bang Gap Energy E_g, eV
300	1.03
473	1.05
623	1.23

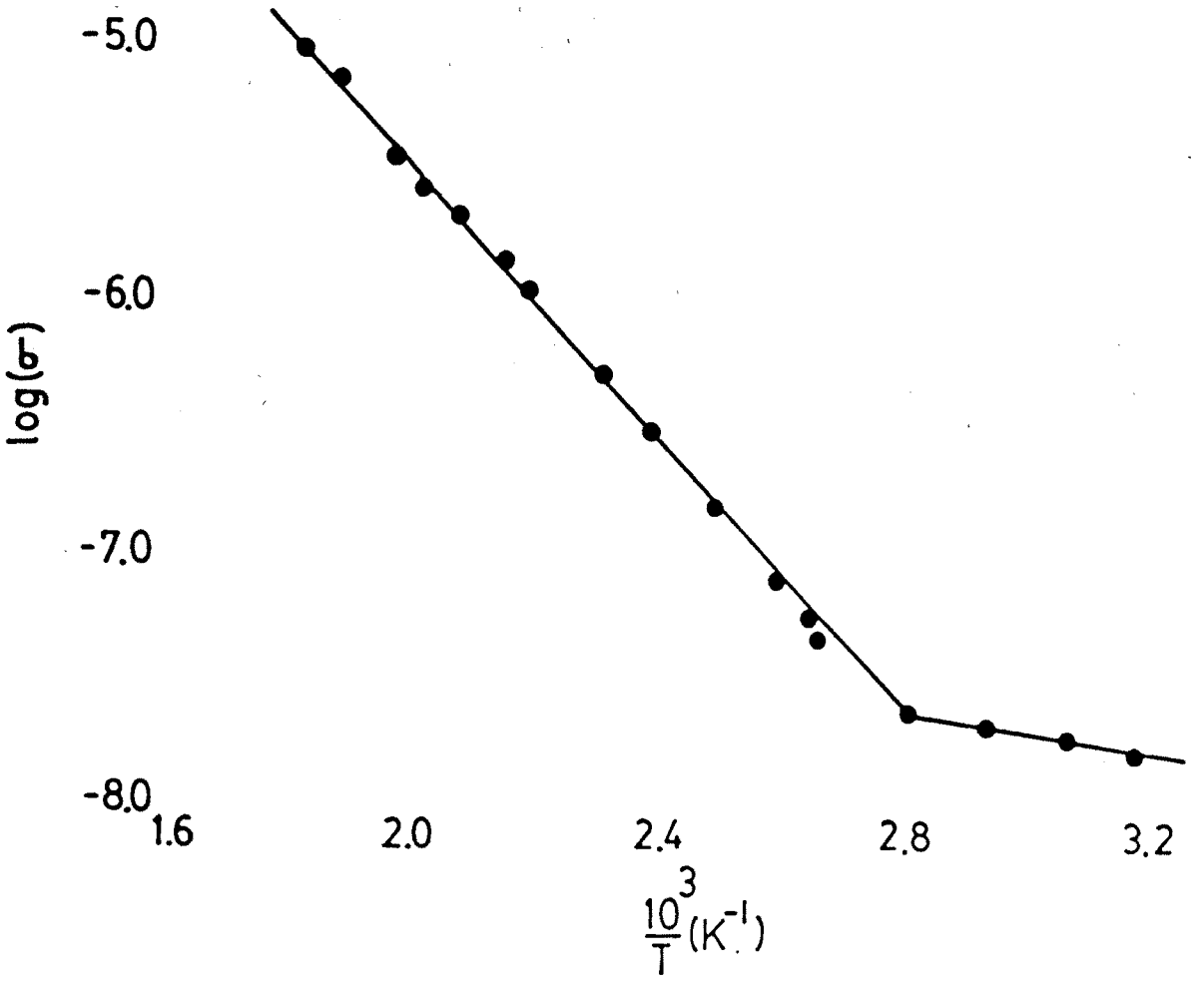

Fig. 3.1 Variation of log σ with (1/T) for InSe thin films.

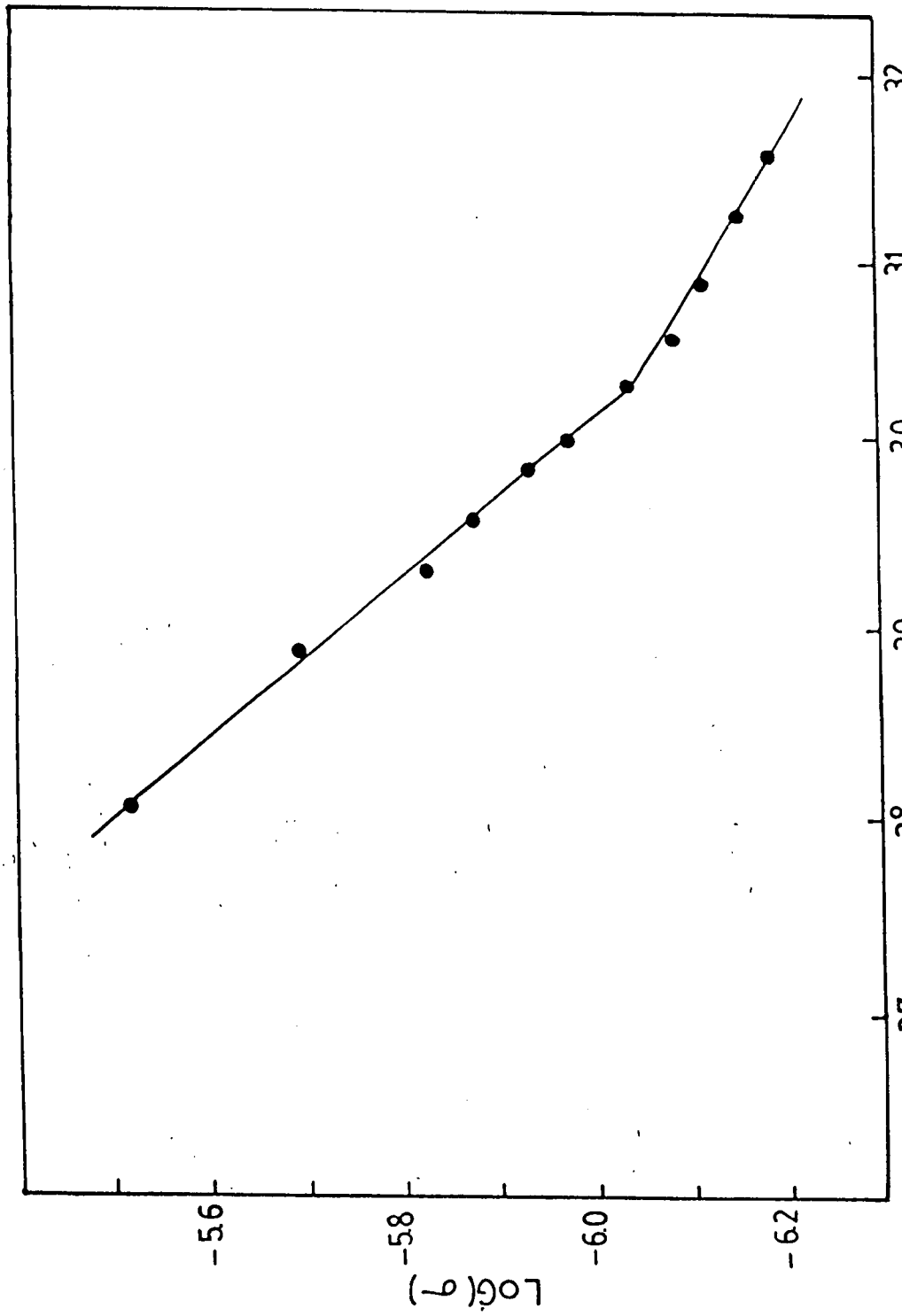

Fig. 3.2 Variation of log σ with (1/T) for InTe thin films.

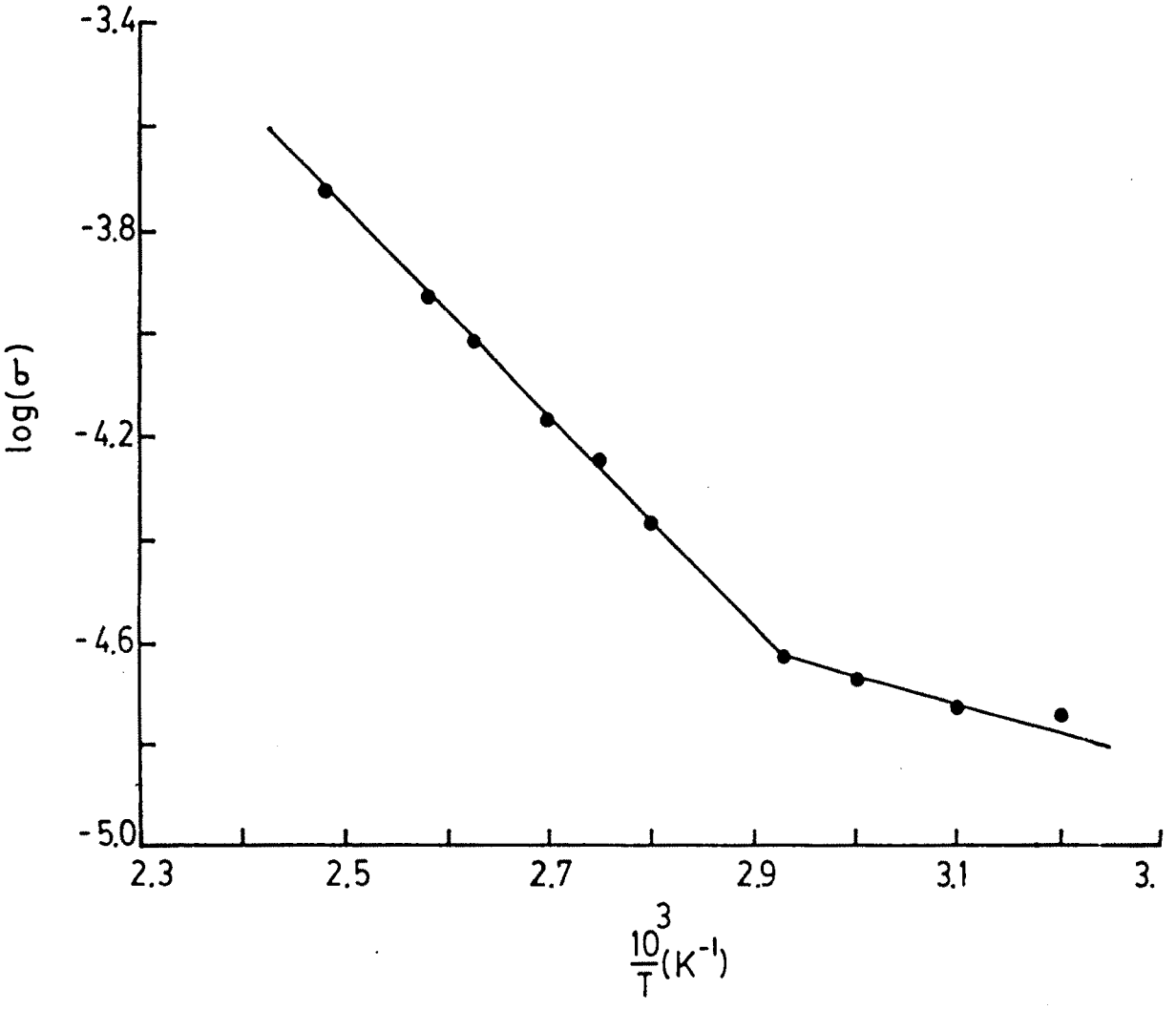

Fig. 3.3 Variation of log σ with (1/T) for In_2Te_3 thin films.

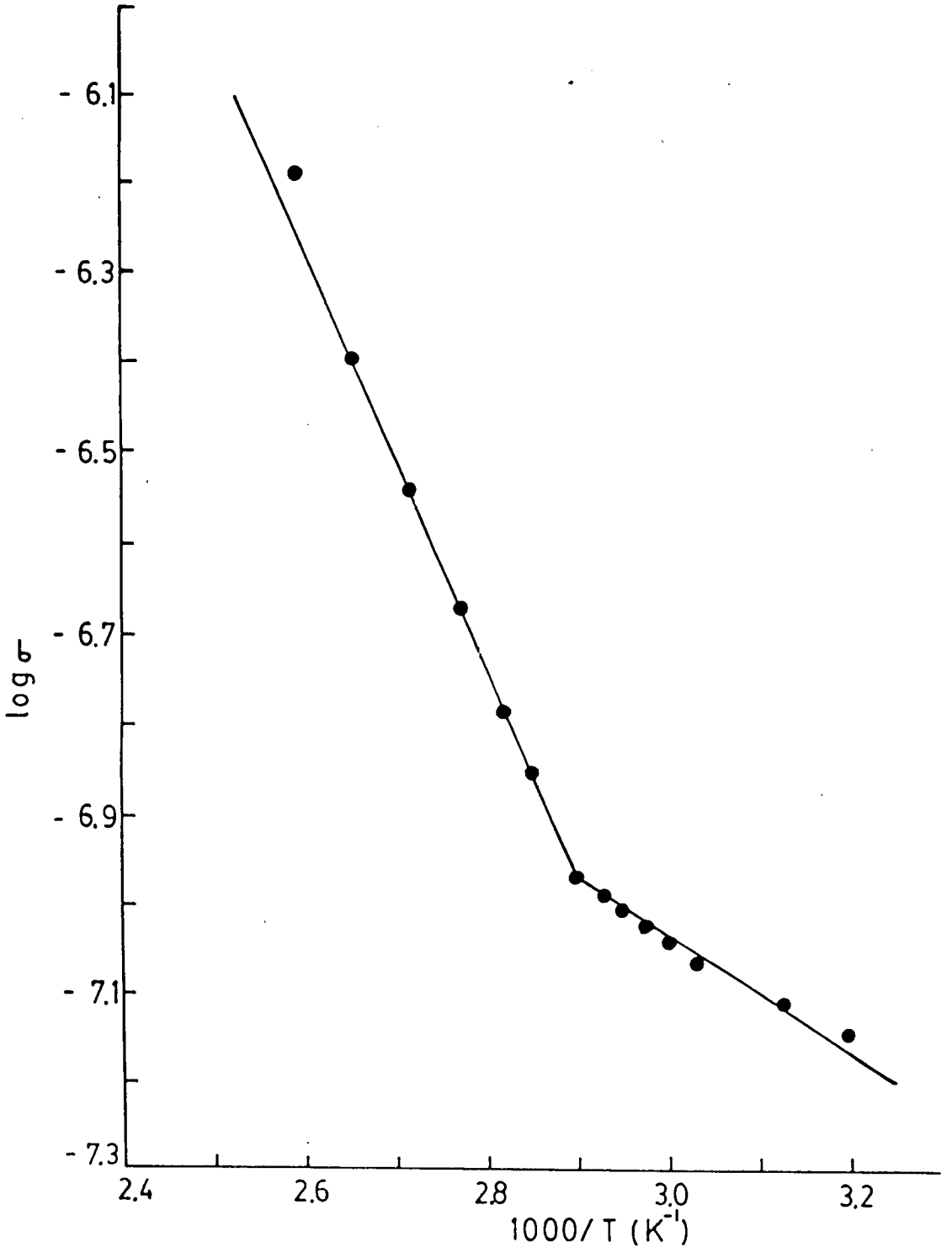

Fig. 3.4 Variation of log σ with (1/T) for $CuInSe_2$ thin films.

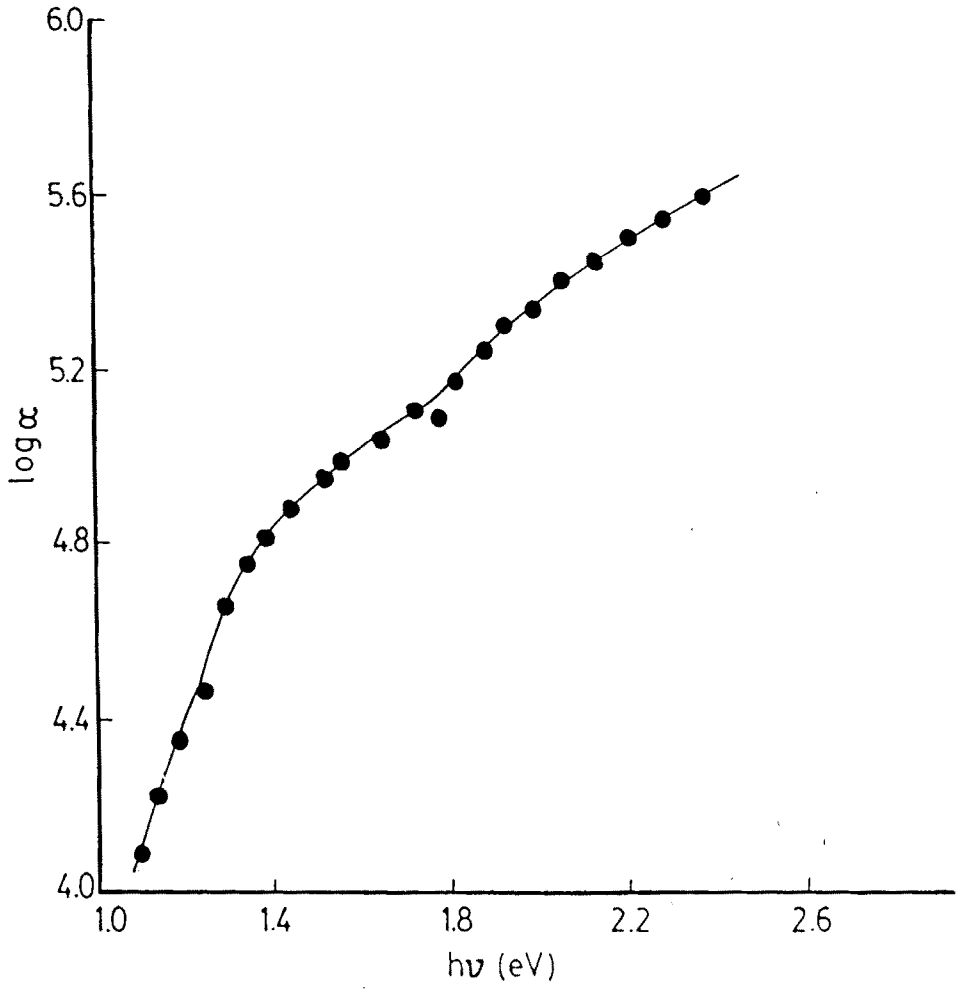

Fig. 3.5 Variation of absorption coefficient with incident photon energy.

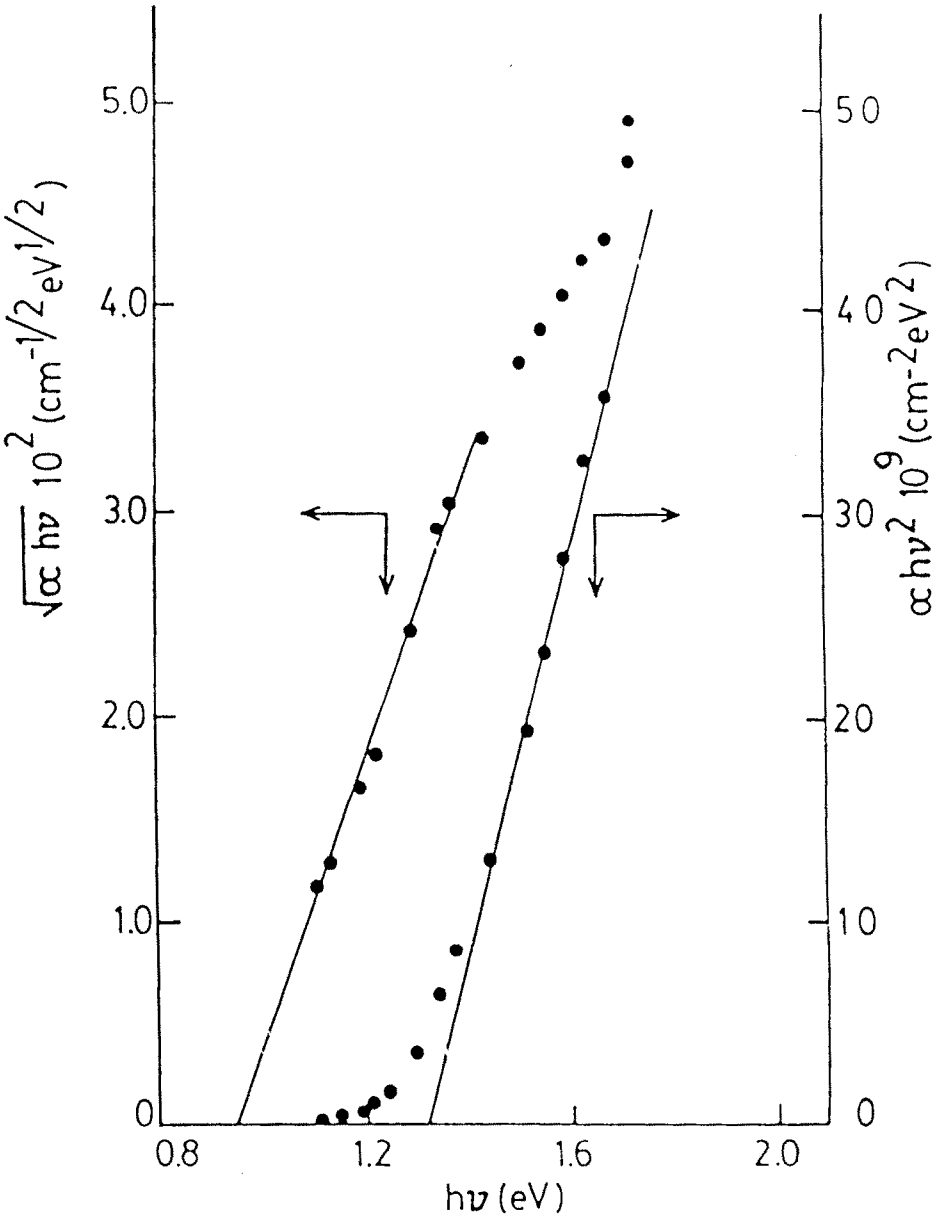

Fig. 3.6 Plots of $(\alpha h\upsilon)^{1/2}$ and $(\alpha h\upsilon)^2$ as a function of incident photon energy $h\upsilon$.

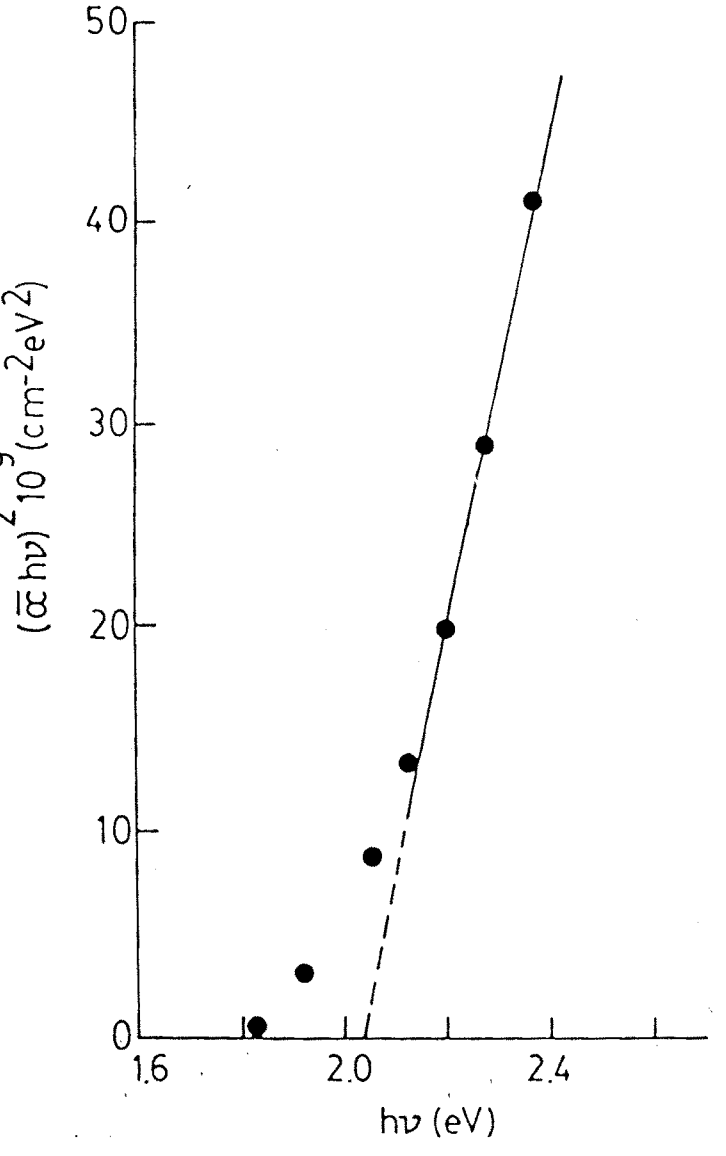

Fig. 3.7 Plot of $(\alpha h\nu)^2$ versus $h\nu$.

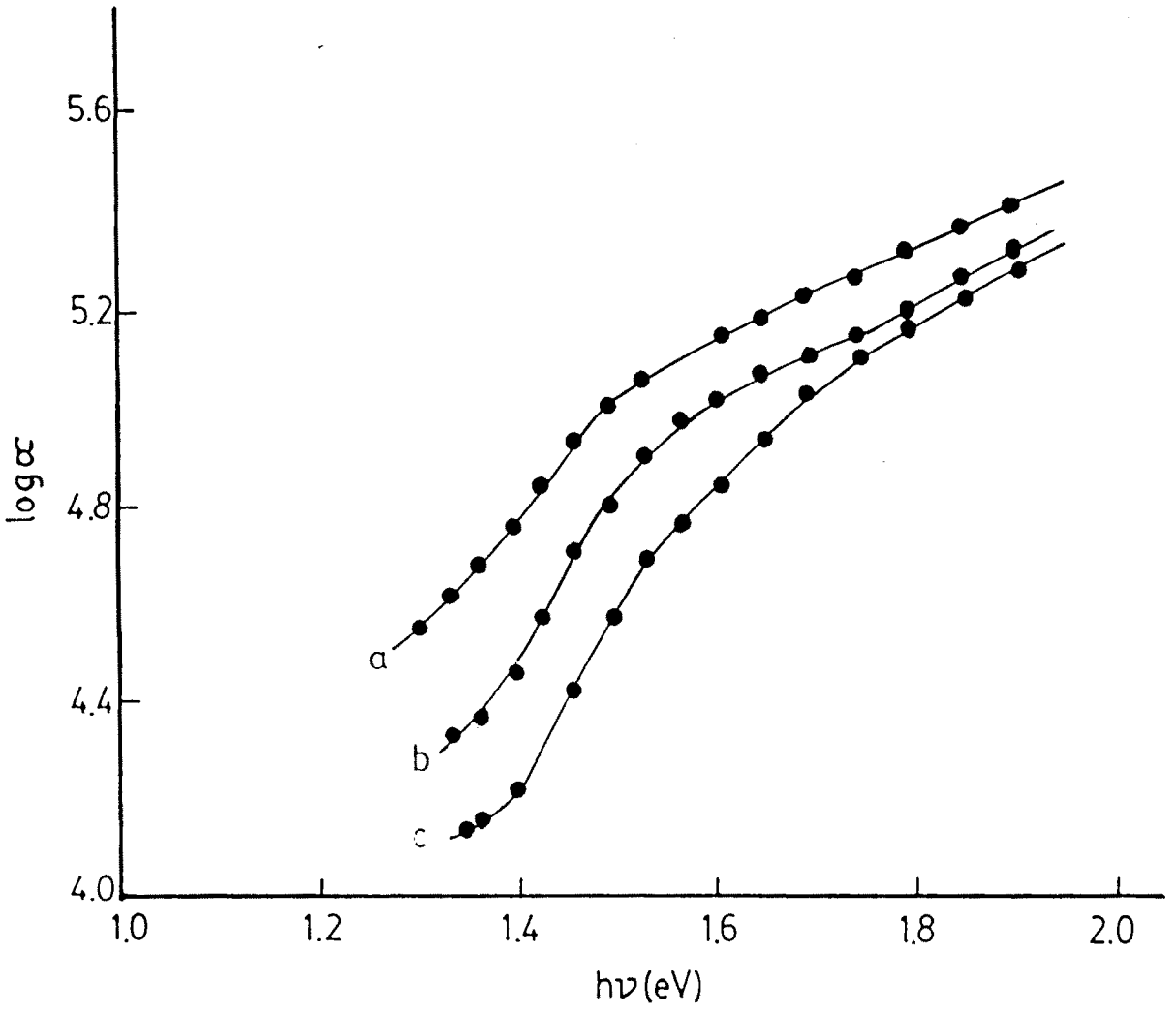

Fig. 3.8 Variation of absorption coefficient with incident photon energy for (a) as-deposited film, (b) film annealed at 423 K & (c) film annealed at 473 K.

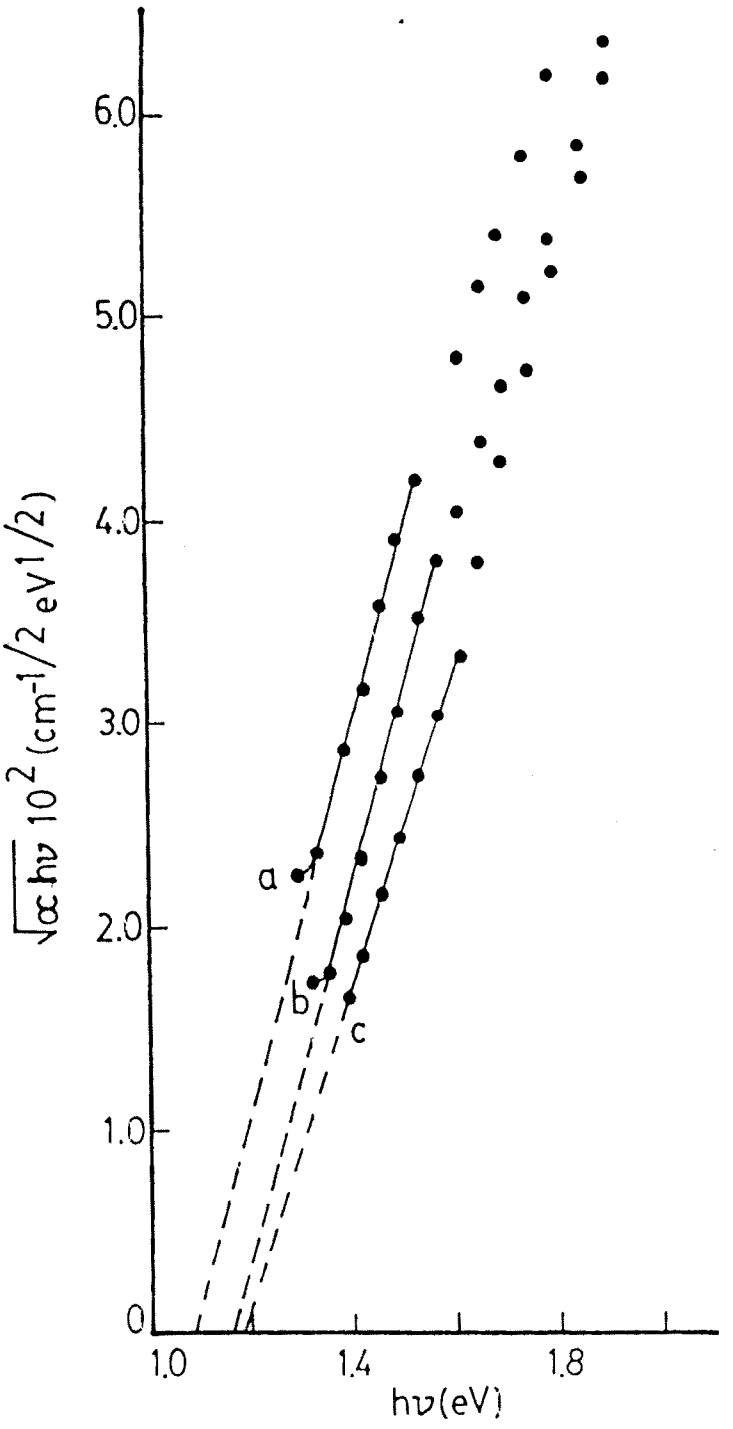

Fig. 3.9 Plots of $(\alpha h\nu)^{1/2}$ as a function of the incident photon energy for (a)as-deposited film (b) film annealed at 423 K and (c) film annealed at 463 K.

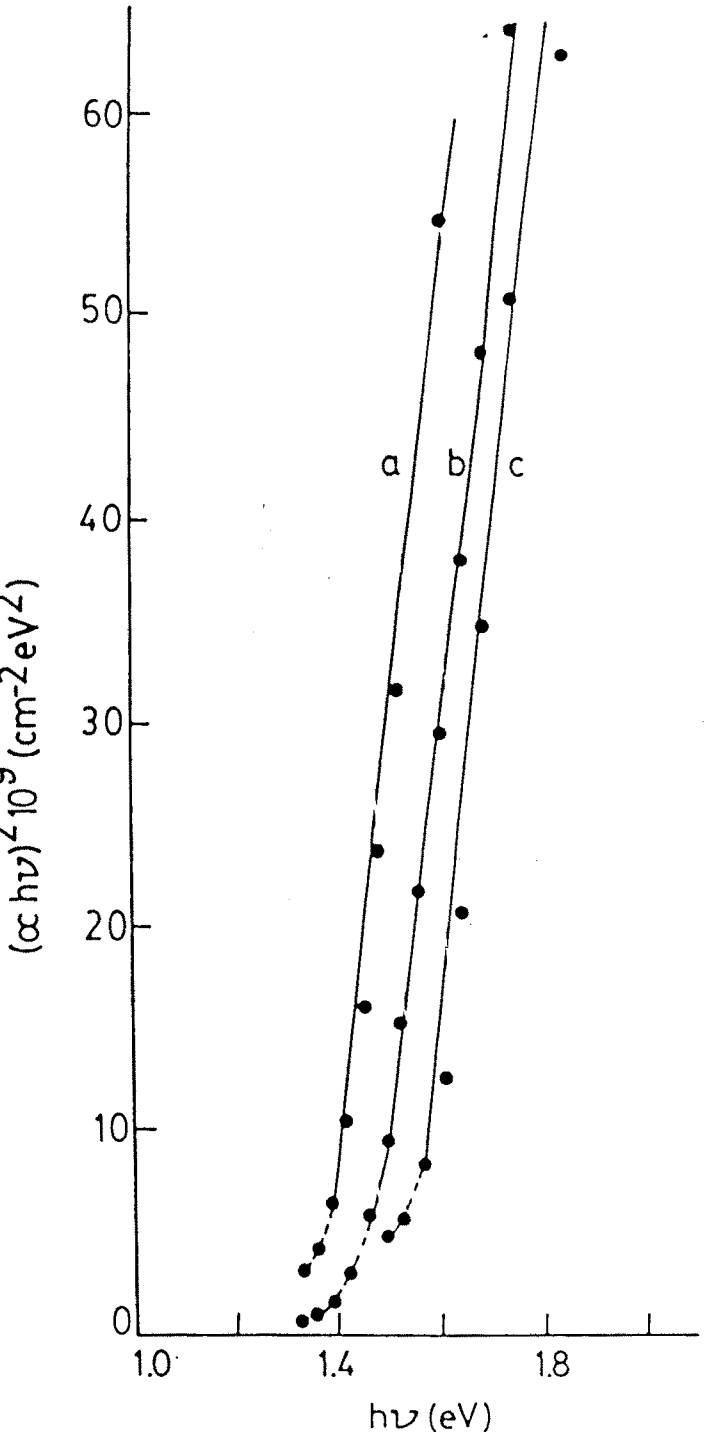

Fig. 3.10 Plot of $(\alpha h\nu)^2$ versus $h\nu$ for (a)as-deposited film, (b) film annealed at 423 K and (c) film annealed at 473 K.

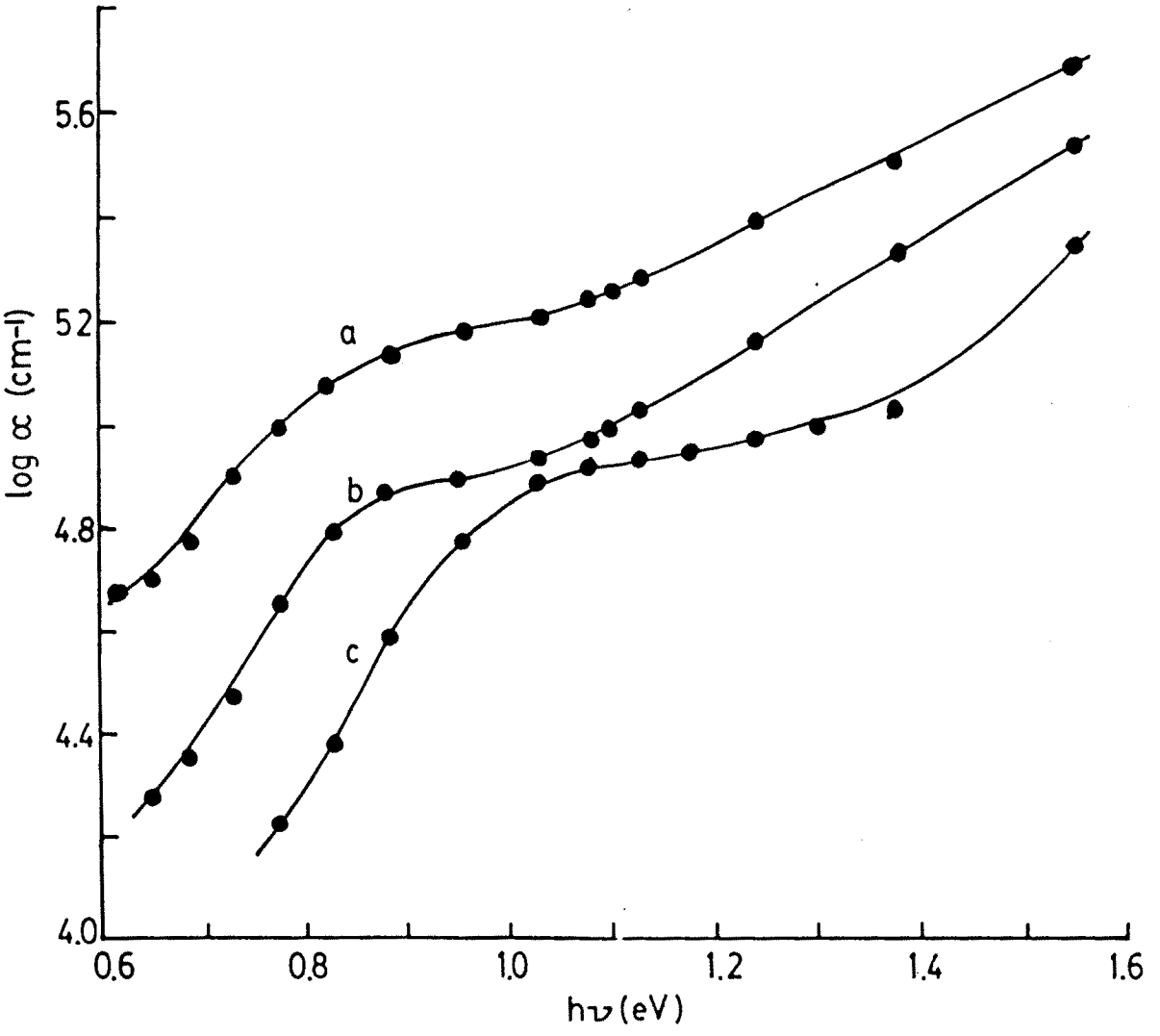

Fig. 3.11 Variation of absorption coefficient of InTe with incident photon energy for (a) as-deposited film, film annealed at (b) 473 K, (c) 573 K.

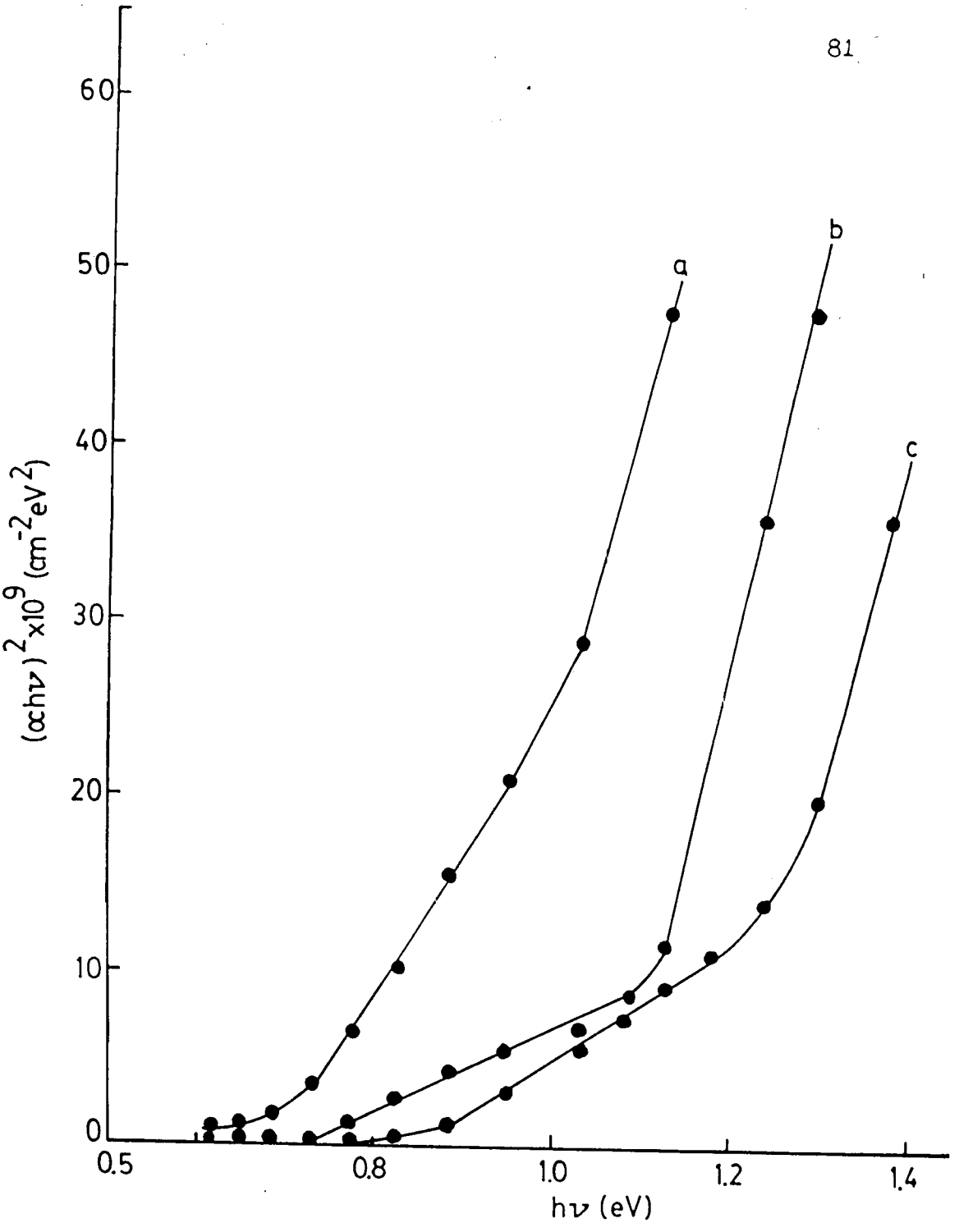

Fig. 3.12 Plots of $(\alpha h\nu)^2$ versus $h\nu$ for (a) as-deposited film, film annealed at (b) 473 K and (c) 573 K.

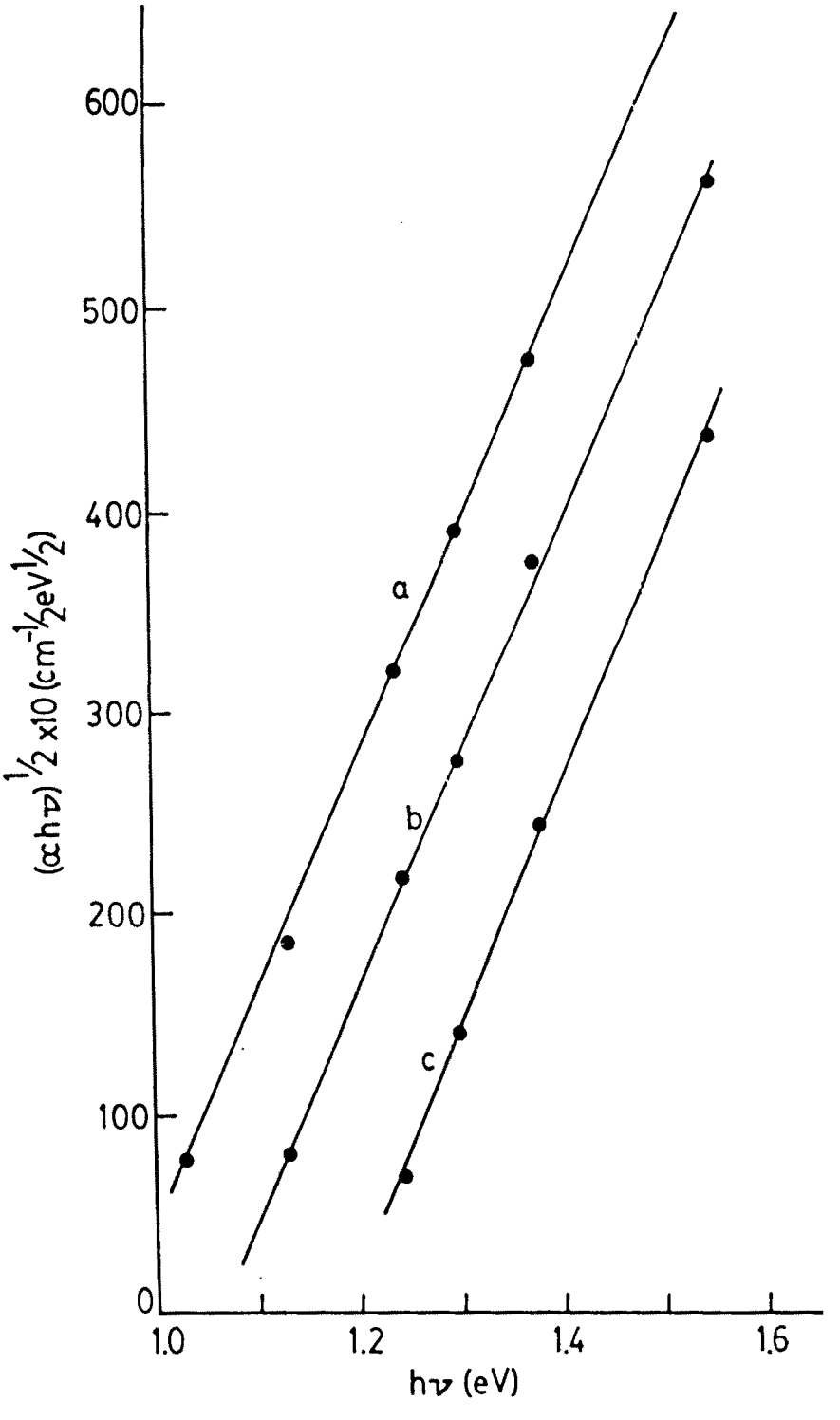

Fig. 3.13 Plots of $(\alpha h\nu)^{1/2}$ versus $h\nu$ for (a) as-deposited film, film annealed at (b) 473K and (c) 573 K.

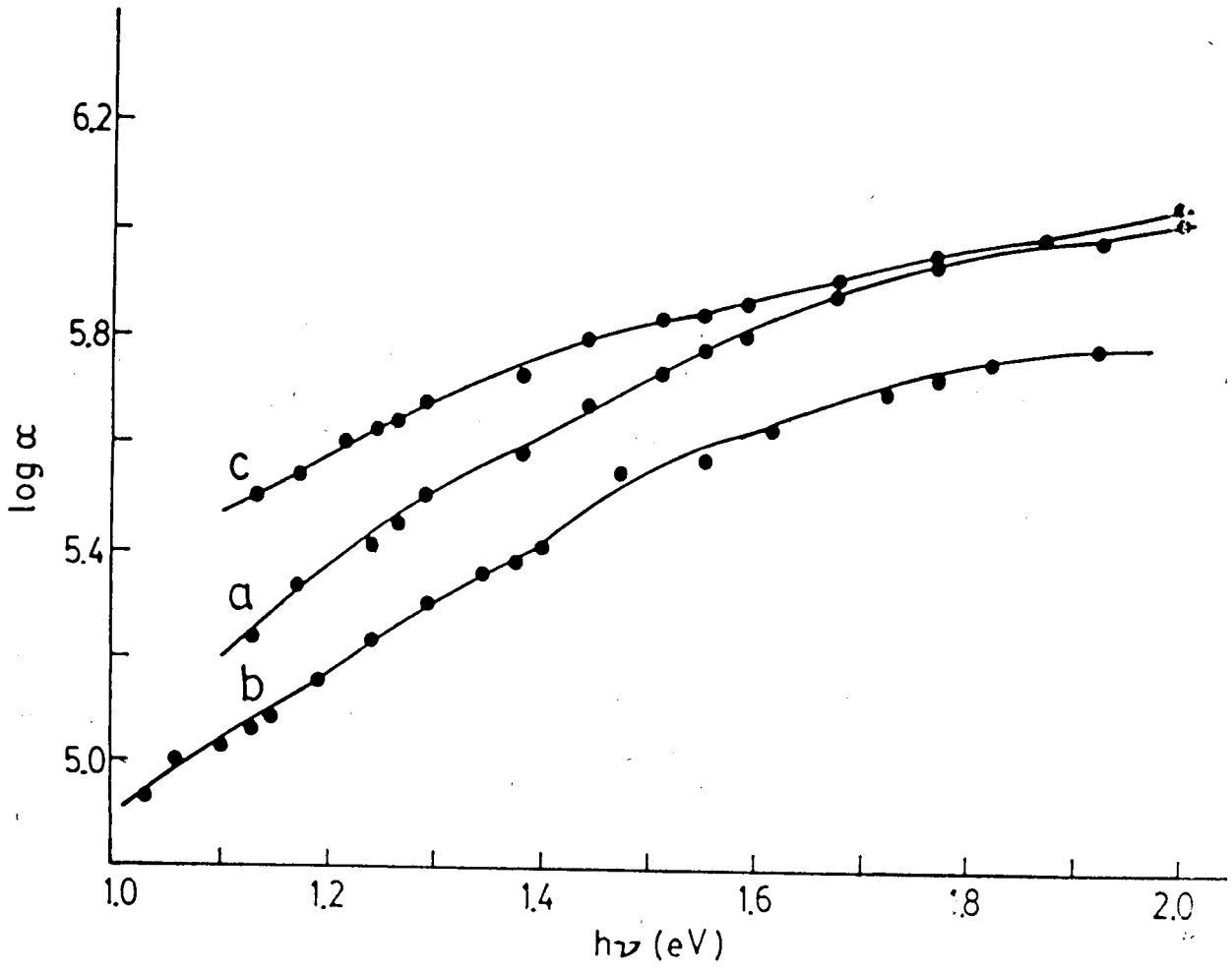

Fig. 3.14 Variation of absorption coefficient of InTe with incident photon energy for film deposited at (a) 373 K, (b) 473 K, and (c) 573 K.

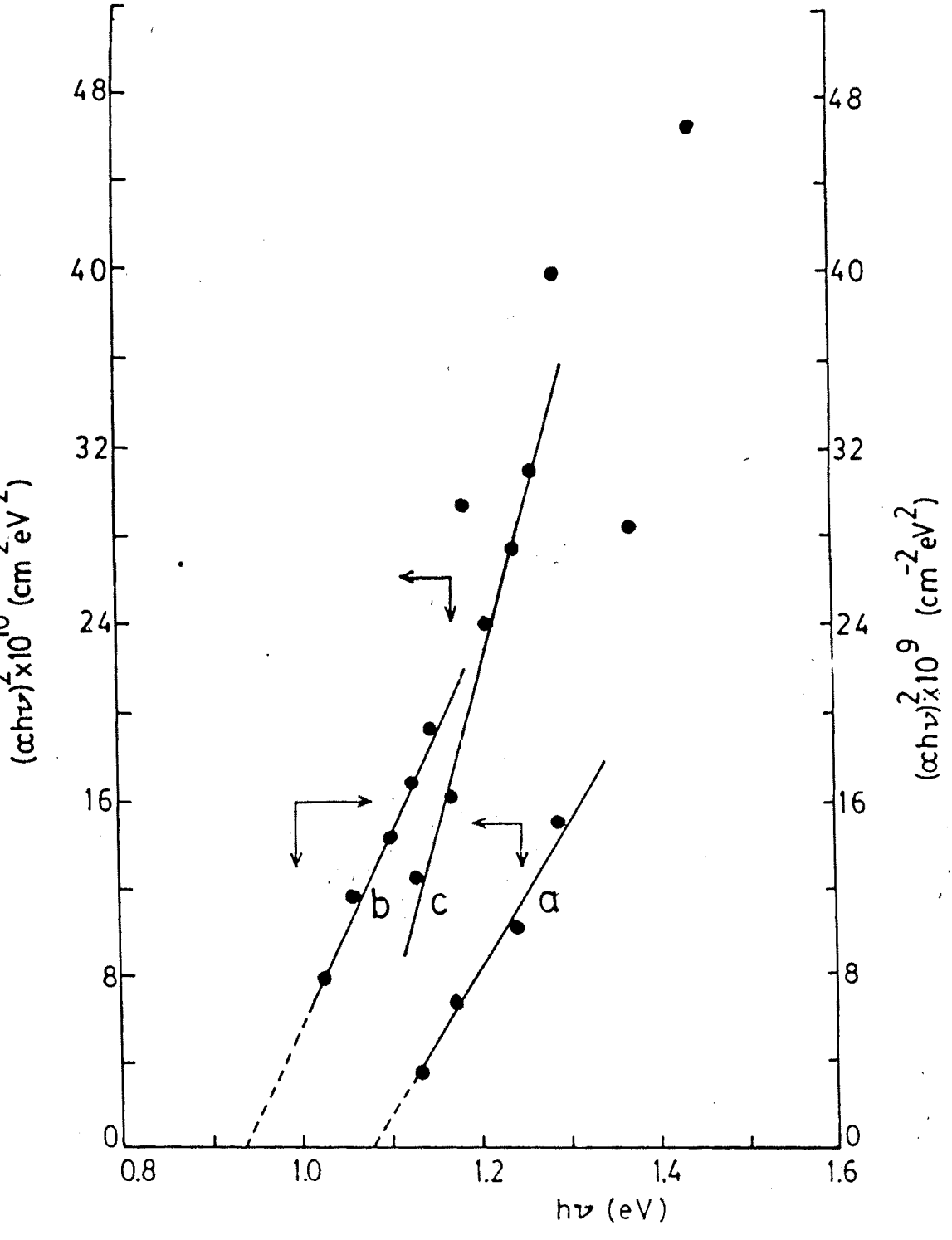

Fig. 3.15 Plots of $(\alpha h\nu)^2$ versus $h\nu$ for film deposited at (a) 373 K, (b) 473 K, and (c) 573 K.

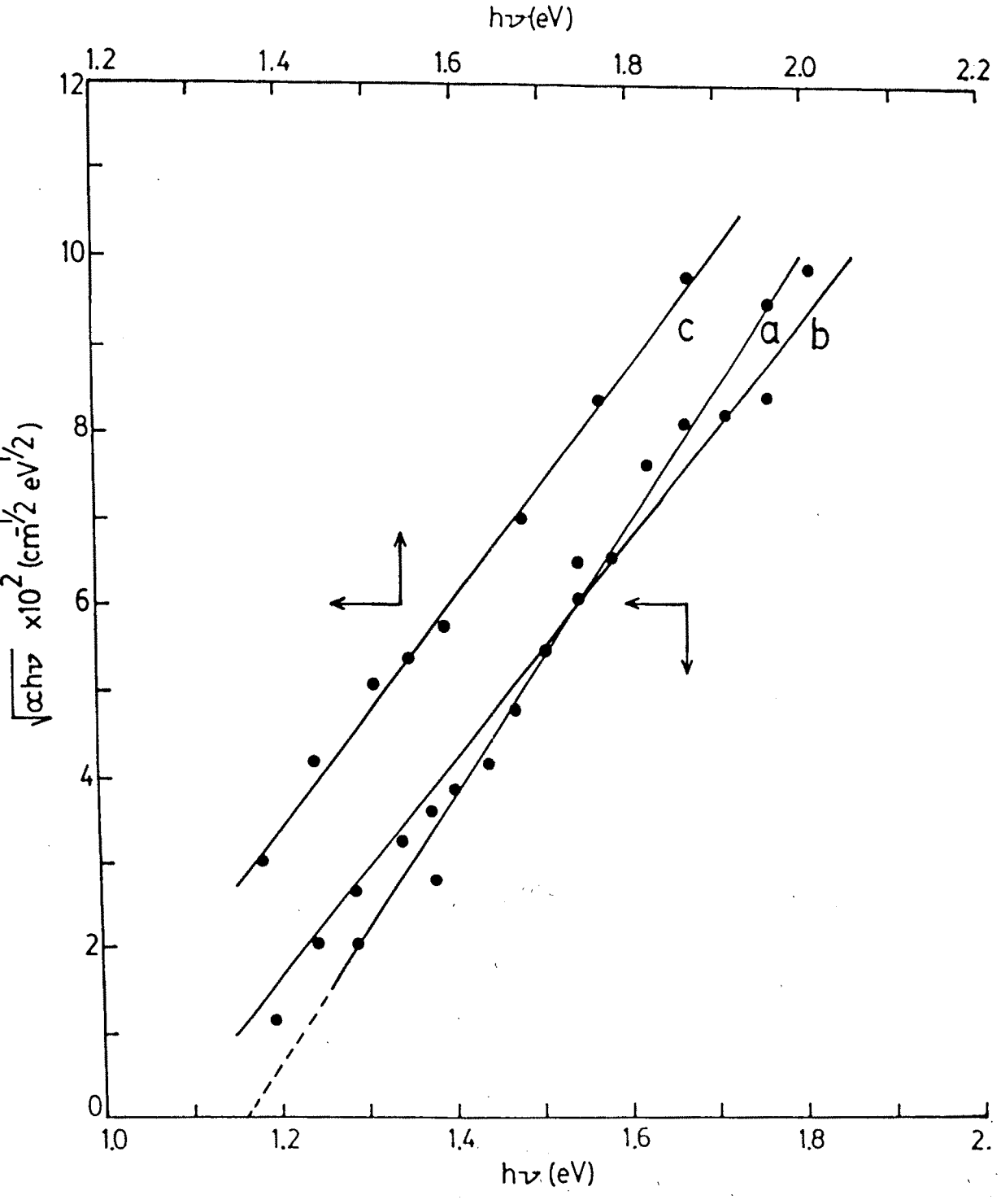

Fig. 3.16 Plots of $(\alpha h\upsilon)^{1/2}$ versus $h\upsilon$ for film deposited at (a) 373 K, (b) 473 K, and (c) 573 K.

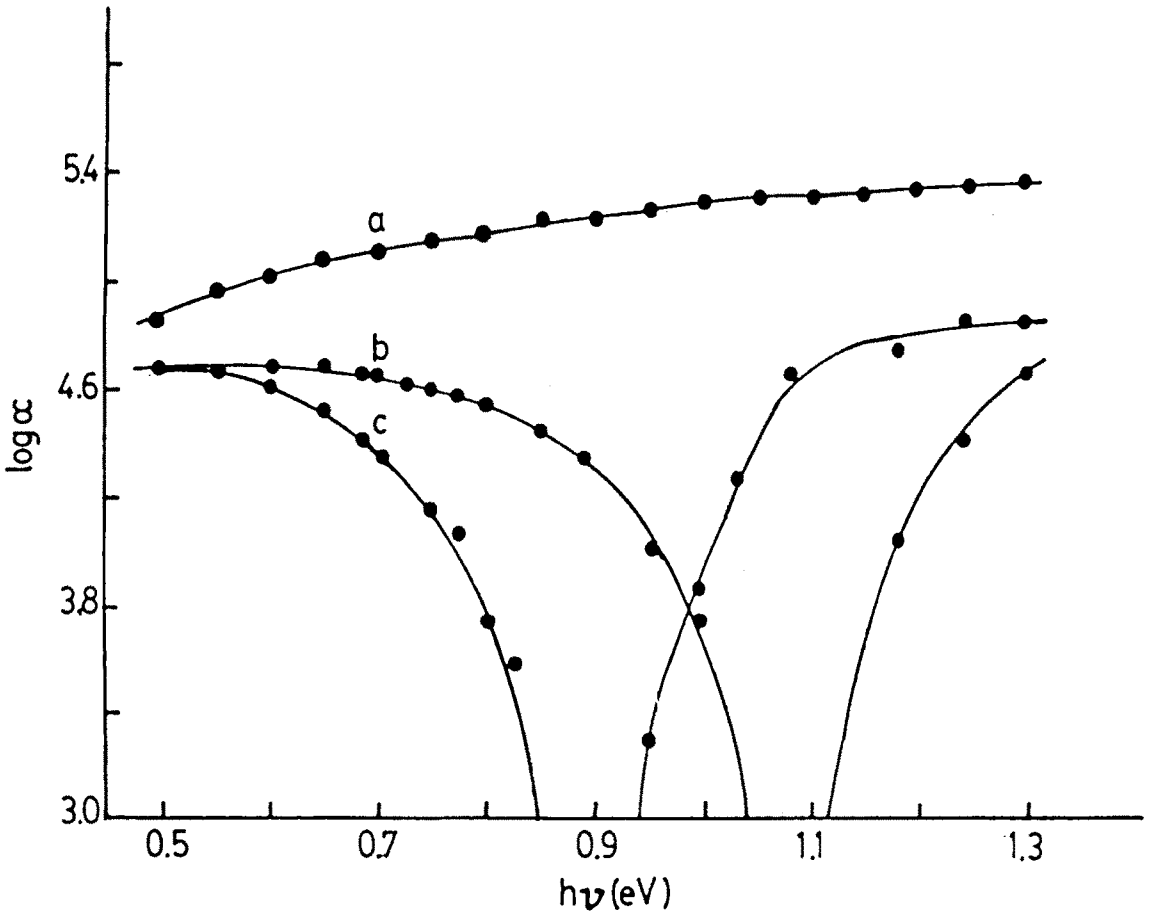

Fig. 3.17 Variation of absorption coefficient with incident photon energy for (a) as-deposited film, (b) film deposited at 473 K, and (c) film deposited at 623 K.

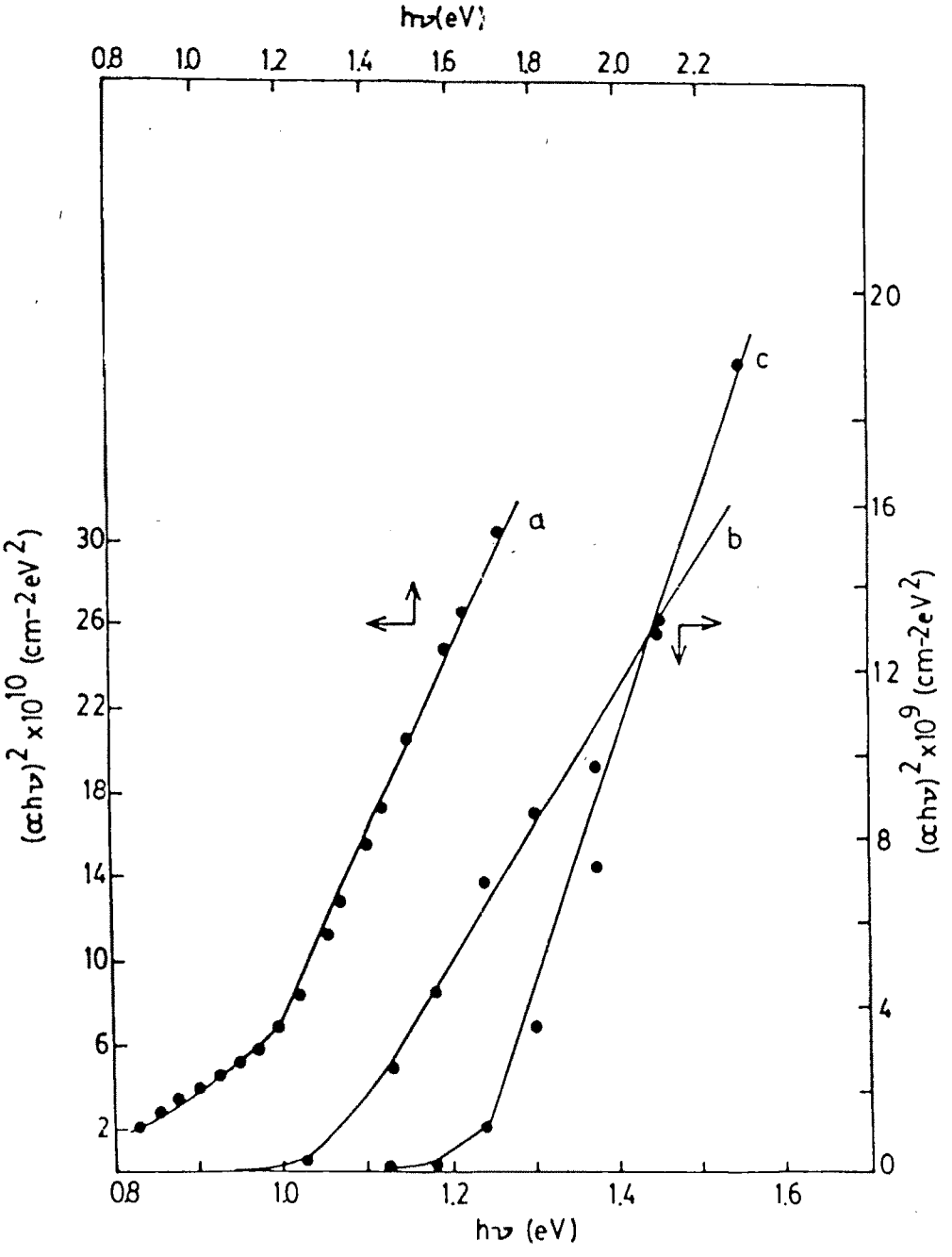

Fig. 3.18 Plots of $(\alpha h\nu)^2$ versus $h\nu$ for (a) as-deposited film, (b) film deposited at 473 K, and (c) film deposited at 623 K.

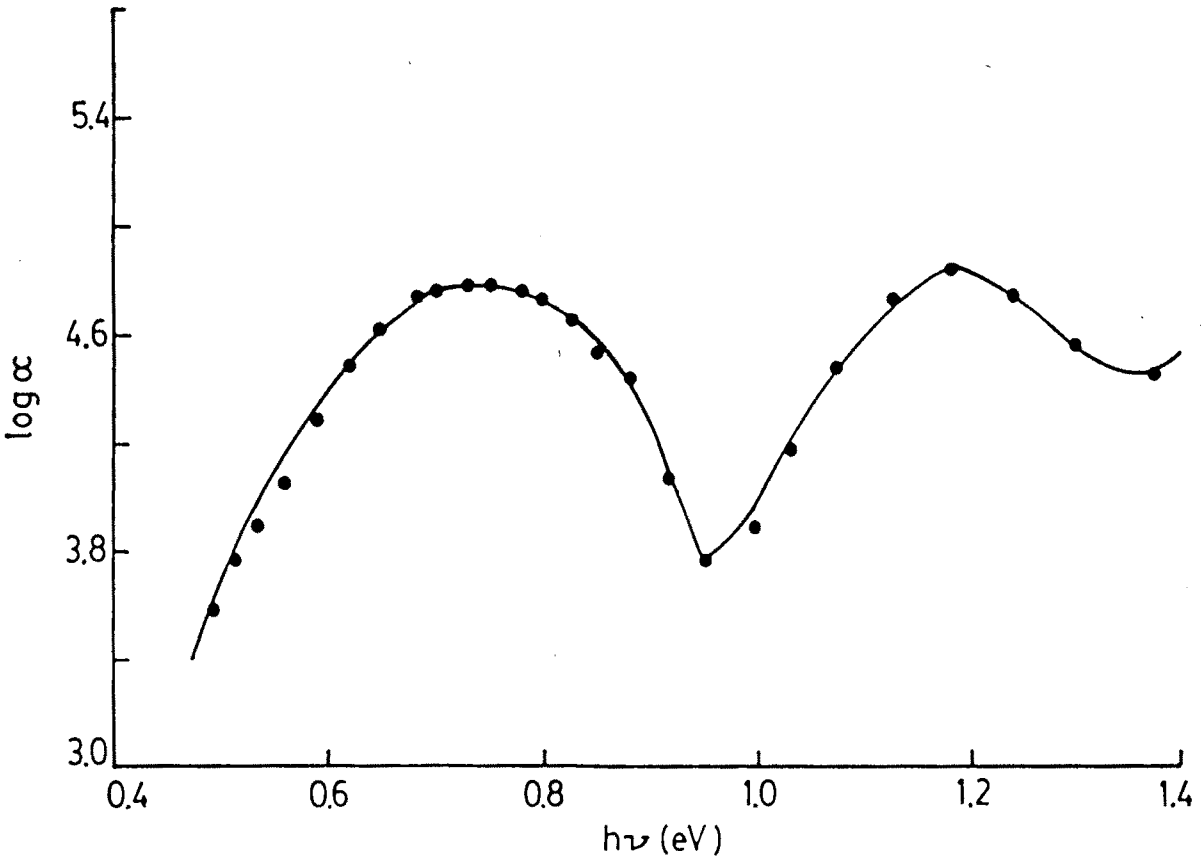

Fig. 3.19 Variation of absorption coefficient of as-deposited $CuInSe_2$ with incident photon energy.

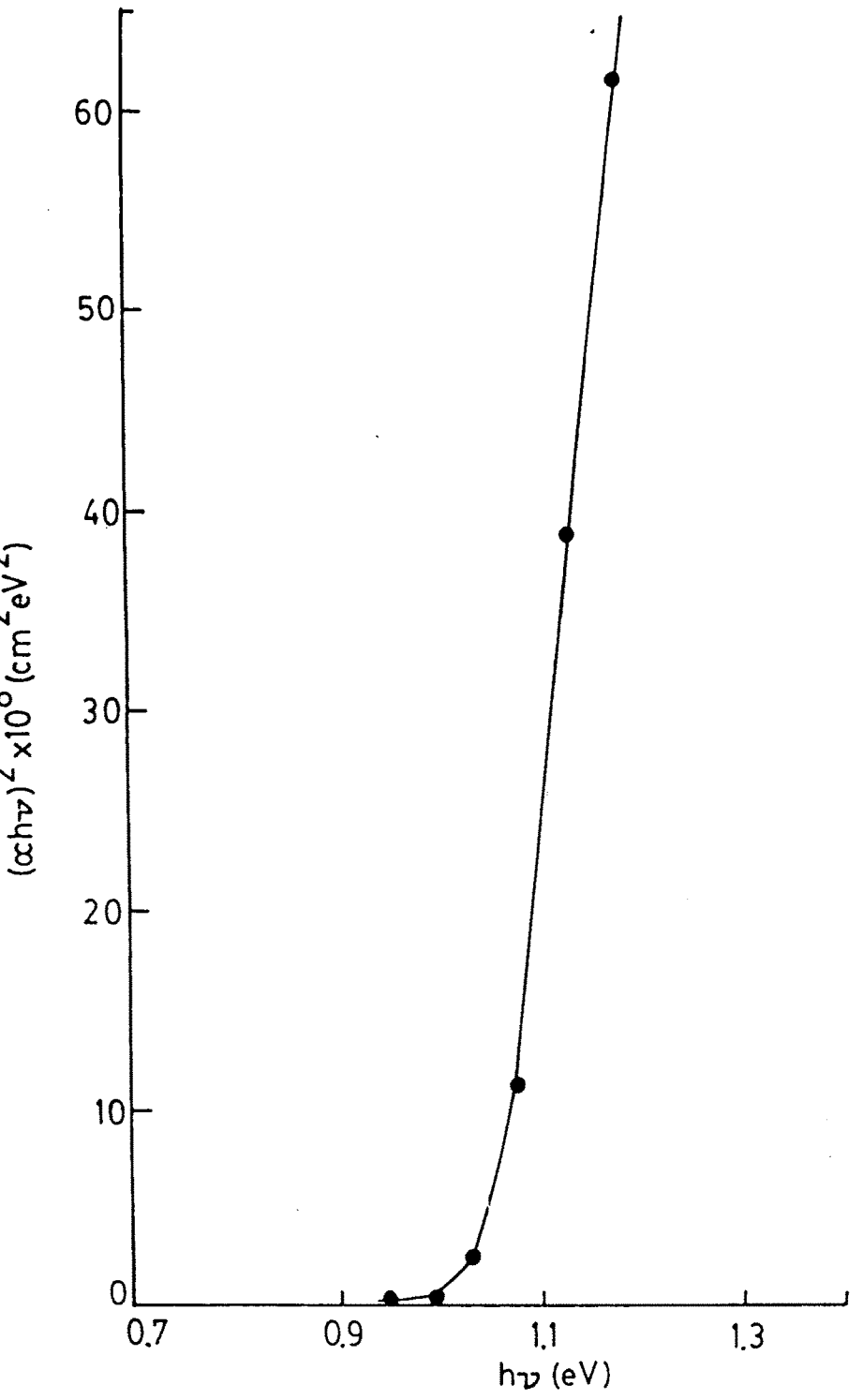

Fig. 3.20 Plots of $(\alpha h\upsilon)^2$ versus $h\upsilon$.

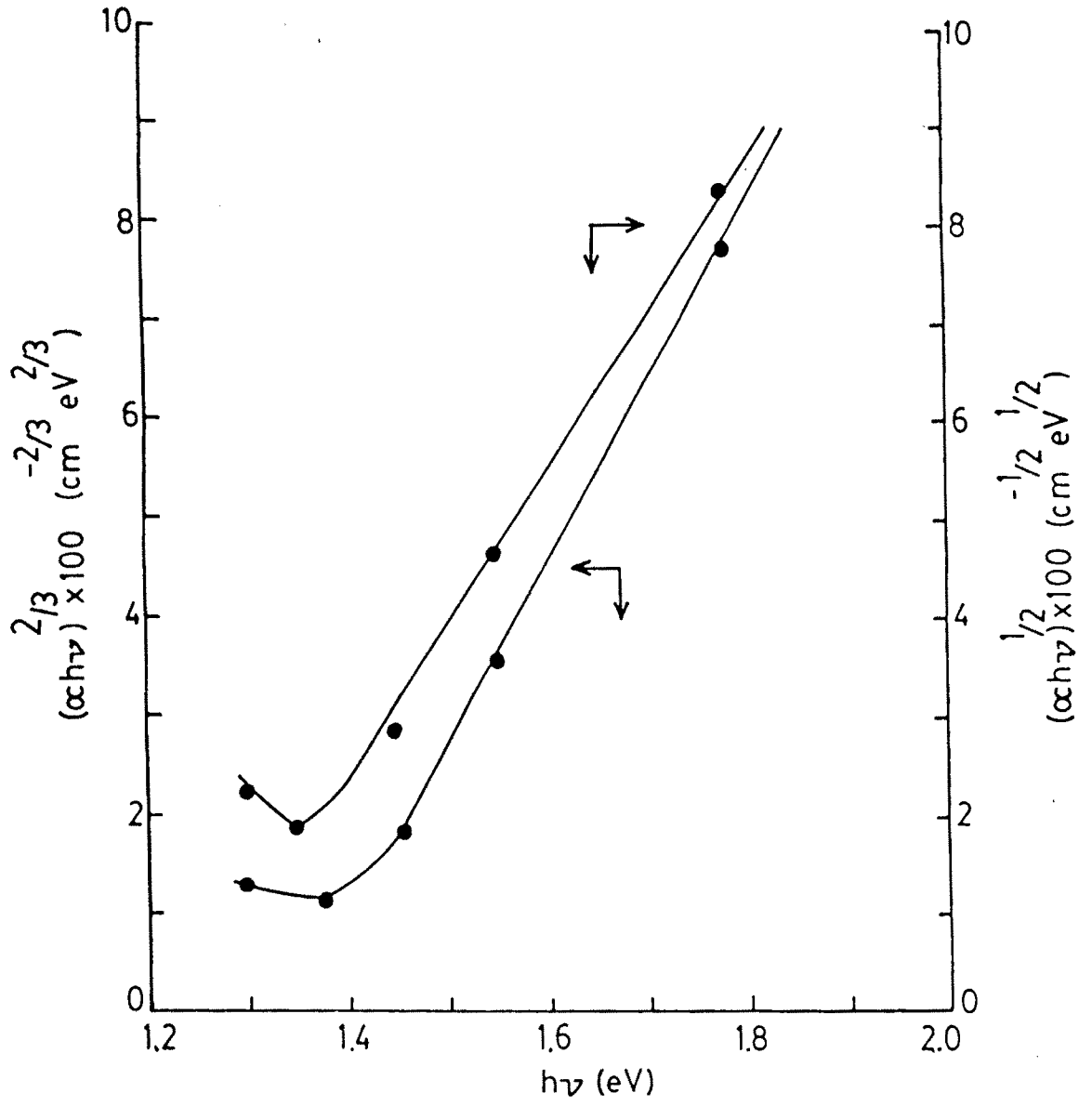

Fig. 3.21 Plots of $(\alpha h\nu)^{1/2}$ and $(\alpha h\nu)^{2/3}$ versus $h\nu$.